

# Coherent Lattice Vibrations in Single-Walled Carbon Nanotubes

Yong-Sik Lim,<sup>†,‡</sup> Ki-Ju Yee,<sup>§</sup> Ji-Hee Kim,<sup>§</sup> Erik H. Házó,<sup>†,#</sup> Jonah Shaver,<sup>†,#</sup> Junichiro Kono,<sup>\*,†,#</sup> Stephen K. Doorn,<sup>⊥</sup> Robert H. Hauge,<sup>#</sup> and Richard E. Smalley<sup>#</sup>

*Department of Electrical and Computer Engineering, Rice University, Houston, Texas 77005, Department of Applied Physics, Konkuk University, Chungju, Chungbuk 380-701, Republic of Korea, Department of Physics, Chungnam National University, Daejeon 305-764, Republic of Korea, Division of Chemistry, Chemical Science & Engineering, Los Alamos National Laboratory, Los Alamos, New Mexico 87545, and Carbon Nanotechnology Laboratory, Rice University, Houston, Texas 77005*

Received July 12, 2006; Revised Manuscript Received September 27, 2006

## ABSTRACT

We have generated and detected coherent lattice vibrations in single-walled carbon nanotubes corresponding to the radial breathing mode (RBM) using ultrashort laser pulses. Because the band gap is a function of diameter, these RBM-induced diameter oscillations cause ultrafast band gap oscillations, thereby modulating the interband excitonic resonances at the phonon frequencies (3–9 THz). Excitation spectra show a large number of pronounced peaks, allowing the determination of the chiralities present in particular samples and relative population differences of particular chiralities between samples.

## Introduction

Electrons, phonons, and their mutual interaction determine most of the properties of crystalline solids.<sup>1</sup> Optical and electrical properties, in particular, are almost entirely dominated by these two fundamental excitations, and it is the subtle interplay between them that gives rise to phenomena such as the Franck–Condon principle and superconductivity. With the advent of ultrafast spectroscopy, one can probe electronic and vibrational dynamics in real time.<sup>2,3</sup> Single-walled carbon nanotubes (SWNTs), with their uniquely simple crystal structures and chirality-dependent electronic and vibrational states, provide a 1D playground for studying the dynamics and interactions of electrons and phonons. Recent continuous wave (CW) optical studies of SWNTs<sup>4–14</sup> have produced a world of intriguing phenomena, including phonon-assisted photoluminescence, strongly bound excitons, and chirality-dependent resonant Raman scattering (RRS), all results of the interaction between excited electronic states and phonons.<sup>15–22</sup>

Here we show the real-time observation of lattice vibrations in SWNTs. Using pump–probe spectroscopy, we observed coherent phonons (CPs) in individualized SWNTs,

corresponding to the radial breathing mode (RBM). The observed RBMs were found to correspond exactly to those seen by CW RRS for the same sample with narrow phonon line widths, no photoluminescence signal or Rayleigh scattering background to obscure features, and excellent resolution, allowing normally blended peaks to appear as distinct features. Additionally, differences in the RBM intensity of particular families of SWNTs were observed between CP spectroscopy and RRS. Finally, when viewing the excitation profiles of several RBMs, we found a two-peak resonance, which we attribute to this technique acting as a modulation spectroscopy; that is, we are observing the first derivative of the interband excitonic absorption peak.

The sample used in this study was a micelle-suspended SWNT solution with a diameter range of 0.7–1.3 nm. The SWNTs (HiP<sub>CO</sub> batch HPR 104) were suspended as individuals with sodium dodecyl sulfate in D<sub>2</sub>O via ultrasonication and centrifugation as previously described.<sup>4</sup> We performed degenerate pump–probe measurements in a quartz cell with an optical path length of 1 mm at room-temperature using ~50 fs pulses from a mode-locked, 89 MHz Ti:Sapphire laser with a bandwidth of ~25 nm and an average pump power of ~20 mW. We tuned the center wavelength in 5-nm steps from 710 to 860 nm (1.75–1.43 eV) by controlling the slit between the intracavity prism pair in the Ti:Sapphire laser. In the CW RRS experiments on the same sample, the excitation source was a CW Ti:Sapphire laser

\* Corresponding author. E-mail: kono@rice.edu.

<sup>†</sup> Department of Electrical and Computer Engineering, Rice University.

<sup>‡</sup> Konkuk University.

<sup>§</sup> Chungnam National University.

<sup>#</sup> Carbon Nanotechnology Laboratory, Rice University.

<sup>⊥</sup> Los Alamos National Laboratory.

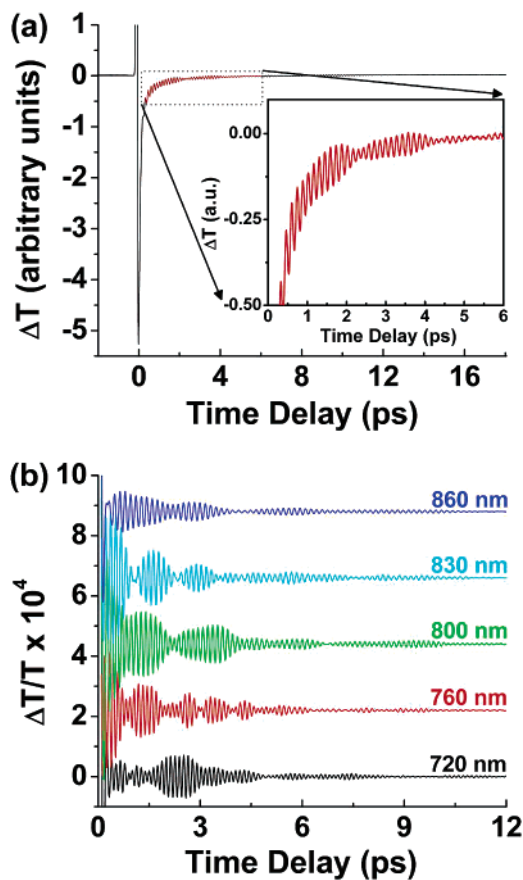


**Figure 1.** (a) Raw pump–probe time-domain data taken at an 800 nm center photon wavelength. The inset is a zoom-in of the data taken between 0.3 and 6 ps, highlighting the CP contribution to the signal. (b) CP oscillations excited and measured at five different photon energies. The individual traces are offset for clarity.

with a power of 15 mW at the sample. Signal collection was done using a triple monochromator and a CCD camera.

Figure 1a is a typical example of the raw pump–probe data taken on our SWNT sample at an 800 nm center photon wavelength. Here, the large electronic contribution is seen at time-zero along with the weaker decaying oscillatory component seen just after, which is attributed to the CP contribution. Figure 1b shows CP oscillations in SWNTs excited at different pump photon energies. The amplitude of oscillations in terms of normalized differential transmission was  $\sim 10^{-4}$  near zero delay. Each trace consists of a superposition of multiple oscillation modes with different frequencies, exhibiting a strong beating pattern. The beating pattern sensitively changes with the photon energy, implying that the CP oscillations are dominated by RBMs, which are resonantly enhanced by pulses commensurate with their unique electronic transitions, as is the case in CW Raman scattering. The decay time of the dominant CP oscillations was  $\sim 5$  ps.

To determine the frequencies of the excited lattice vibrations, we took a fast Fourier transform (FFT) of the time-domain oscillations to produce CP spectra (Figure 2a). For comparison, we show CW RRS spectra (Figure 2b) for the same sample. The CP spectra (Figure 2a) are seen to cluster into three distinct regions, similar to CW RRS,<sup>7</sup> as shown

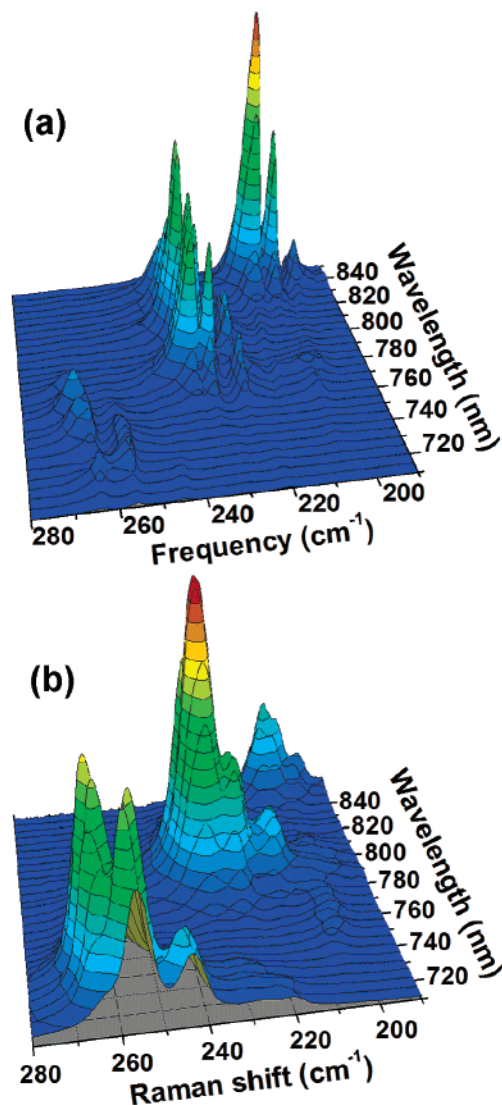


**Figure 2.** (a) A 3D plot of the FFT of CP oscillations obtained over a photon energy range of 710–850 nm (1.746–1.459 eV) with a 5-nm step size. (b) A 3D plot of RRS over an excitation energy range of 710–850 nm (1.746–1.459 eV) with a 5-nm step size.

in Figure 2b. The main peak positions coincide between panels a and b of Figure 2, indicating that the oscillations seen in Figure 1b are indeed due to the RBM of coherent lattice vibrations. However, upon close examination, we find a few noticeable differences between the CP data and the CW RRS data: (i) unresolved shoulder features in RRS are seen as clear peaks in the CP spectra due to the narrow line widths, (ii) there are different intensity distributions among the strongest peaks in the three distinct regions, and (iii) the CP spectra show a surprising double-peak dependence on the photon energy.

Figures 3 a–c present a direct comparison between CP spectra and CW RRS spectra. Here, the CP spectra obtained with different wavelengths are overlaid onto the equivalent RRS spectra taken at the same wavelengths of 710 nm (1.746 eV), 765 nm (1.621 eV), and 830 nm (1.494 eV), respectively. There is overall agreement between the two spectra in each figure. However, it is clear that several features are

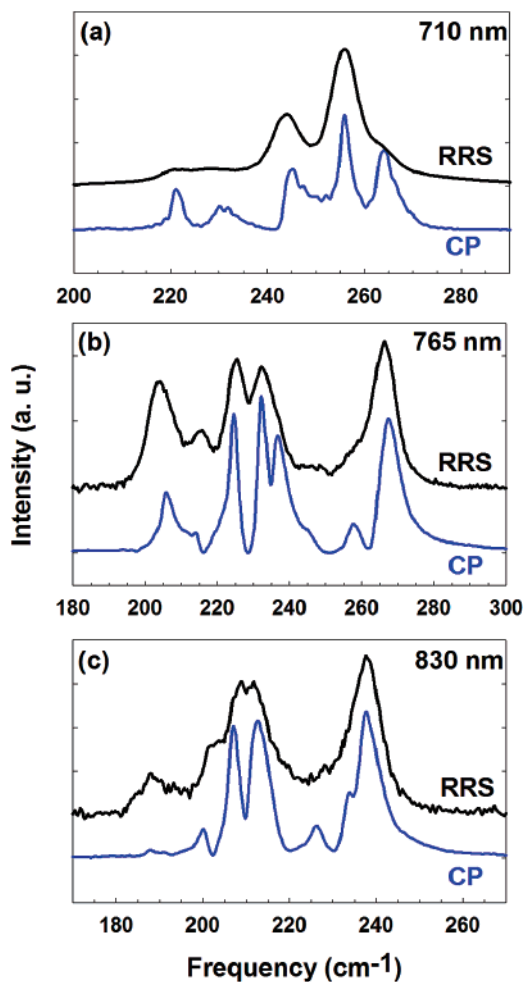


**Figure 3.** Phonon spectra using three different photon energies obtained from RRS and CP measurement. The traces are offset for clarity.

more resolved in the CP data. The narrower line widths in the CP data make it possible to resolve blended peaks in the RRS data. With less overlap among the close-by peaks, more precise determination of line positions is possible. Through peak fitting using Lorentzians, we have identified and successfully assigned 18 RBMs in the CP spectra over the 1.44–1.75 eV (710–860 nm) photon energy range with an average measured line width of  $\sim 3 \text{ cm}^{-1}$ . Line widths measured in this study for HiP<sub>CO</sub> material using CW RRS and in other high-resolution CW RRS experiments for different carbon nanotube samples<sup>13,14,19,23–28</sup> were consistently 5–6  $\text{cm}^{-1}$ ; the two notable exceptions are isolated SWNTs suspended over a trench<sup>29</sup> and the inner shell tube of double-walled carbon nanotubes (DWNTs)<sup>23,24</sup> where RRS measured 1.5 and 1  $\text{cm}^{-1}$  line widths, respectively. Previous studies on CPs in semiconductors,<sup>30–32</sup> large organic dye molecules,<sup>33–35</sup> bulk metal films<sup>36</sup> and metal nanoparticles and nanorods<sup>37</sup> indicate general agreement with phonon line widths obtained by CW RRS, although, in some cases, line widths measured were greater than or less than the RRS line width. In both CP spectroscopy and RRS, the primary decay process of phonons is most likely to be through disappearance into lower-frequency phonon modes by anharmonicity.<sup>3,32</sup> However, other broadening mechanisms such as interactions

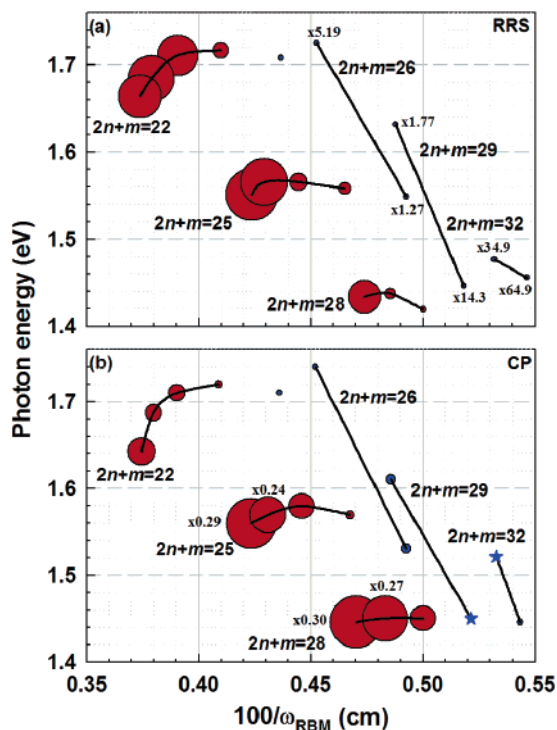


**Figure 4.** (a) Raman intensity and (b) CP signal as a function of excitation energy and  $100/\omega_{\text{RBM}}$ , where  $\omega_{\text{RBM}}$  is the phonon frequency. Red (blue) circles denote nanotubes that satisfy  $(n-m) \bmod 3 = -1 (+1)$ . The black lines connect members of the same  $(2n+m)$  family. The diameter of the circles is proportional to measured intensities.<sup>27</sup> The blue stars in panel b indicate chiralities with large uncertainty in their determined excitonic energies and CP signal.

with the environment and intertube interactions should be studied as well as temperature dependence to identify the exact decay mechanism.

Figure 4 summarizes the observed RBMs both from CW Raman scattering (Figure 4a) and CPs (Figure 4b).<sup>38</sup> The dependence of CP signal strength as a function of photon energy and phonon frequency exhibits several of the same trends both predicted theoretically<sup>17–22</sup> and measured experimentally<sup>7,14</sup> by CW Raman scattering for intensity as a function of excitation energy and Raman shift. When exciting the second excitonic transition for an individual semiconducting SWNT,  $E_{22}$ ,  $(n-m) \bmod 3 = -1$  nanotubes have markedly stronger signals than  $(n-m) \bmod 3 = +1$  nanotubes. Additionally, within a  $(2n+m)$  nanotube family, signal strength increases from nanotubes with large or near  $30^\circ$  chiral angles (near-“armchair”) to nanotubes with small or  $0^\circ$  chiral angle (“zigzag”). Both observed behaviors stem from the proportionality of the RRS/CP intensity to the square of the electron–phonon coupling matrix element, whose magnitude possesses both a mod type and chiral angle dependence.<sup>7,14,17,19–22,39</sup> However, the two techniques differ when comparing the overall signal strength. Namely, in Raman scattering, signal strength decreases as  $(2n+m) = \text{constant}$  increases, whereas CP signal increases with increasing  $(2n+m) = \text{constant}$ . We currently have no theoretical model to explain this striking difference between CP measurements and RRS, and it is thus open for further studies.

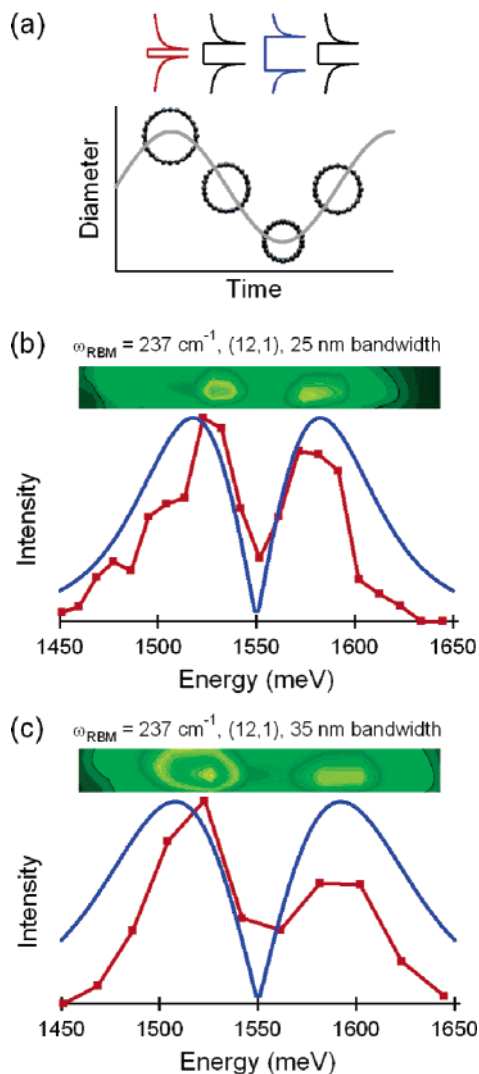


**Figure 5.** (a) Time-dependent band gap due to the RBM of coherent lattice oscillations. (b,c) The photon energy dependence of the CP signal intensity (both contour and 2D plots) for the (12,1) tube with a probe bandwidth of (b) 25 nm and (c) 35 nm, together with theoretical curves (blue solid lines).

Finally, we discuss how the generation of CPs of RBMs modifies the electronic structure of SWNTs and how it can be detected as temporal oscillations in the transmittance of the probe beam. The RBM is an isotropic vibration of the nanotube lattice in the radial direction, that is, the diameter ( $d_t$ ) periodically oscillates at frequency  $\omega_{\text{RBM}}$ . This causes the band gap  $E_g$  to also oscillate at  $\omega_{\text{RBM}}$  (see Figure 5a) because  $E_g$  directly depends on the nanotube diameter (roughly  $E_g \propto 1/d_t$ ). As a result, interband transition energies oscillate in time, leading to ultrafast modulations of optical constants at  $\omega_{\text{RBM}}$ , which naturally explains the oscillations in probe transmittance. Furthermore, these modulations imply that the absorption coefficient at a fixed probe photon energy is modulated at  $\omega_{\text{RBM}}$ . Correspondingly, the photon energy dependence of the CP signal shows a *derivative-like* behavior, à la modulation spectroscopy<sup>40</sup> (see Figure 5b,c). We modeled this behavior assuming that the CP signal intensity is proportional to the absolute value of the convoluted integral of the first derivative of a Lorentzian absorption line

and a Gaussian probe beam profile. The results, shown as solid lines in Figure 5b,c, successfully reproduce the observed double peaks, whose energy separation changes with the bandwidth of the probe. The *symmetric* double-peak feature confirms the excitonic nature of the absorption line, in contrast to the asymmetric shape expected from the 1D van Hove singularity.

In addition to revealing a novel optical process, involving both 1D excitons and phonons simultaneously, this study opens up a number of new possibilities to study SWNTs. In particular, it has several advantages, including (i) excellent resolution and narrow line widths, (ii) no Rayleigh scattering background at low frequency, (iii) no photoluminescence signal, and (iv) direct measurement of vibrational dynamics, including its phase information and decay times. The excitonic nature of interband optical excitation manifests itself in the detection process for the CP oscillations by the coupling with the broad spectrum of probe pulses. Furthermore, the expansion of the spectrum of femtosecond pulses into the deep mid-infrared and visible ranges will allow us to explore large-diameter carbon nanotubes and metallic carbon nanotubes. Finally, the ability of CP measurements to trace the first derivative of the excitonic absorption peaks of specific chirality ( $n,m$ ) tubes will allow in-depth study of the line shape of these resonances.

**Acknowledgment.** Y.S.L. acknowledges financial support from Konkuk University. This work was supported in part by the Robert A. Welch Foundation (No. C-1509) and NSF (Nos. DMR-0134058 and DMR-0325474). S.K.D. appreciates the support of the LANL Integrated Spectroscopy Laboratory and partial financial support of this work from the LANL LDRD program. We thank Carter Kittrell, Andrew Shreve, and David Hilton for helpful discussions and comments.

## References

- (1) Ziman, J. M. *Electrons and Phonons*; Oxford University Press: Oxford, 1960.
- (2) Shah, J. *Ultrafast Spectroscopy of Semiconductors and Semiconductor Nanostructures*; Springer: Berlin, 1999.
- (3) Merlin, R. *Solid State Comm.* **1997**, *102*, 207.
- (4) O'Connell, M. J.; Bachilo, S. M.; Huffman, C. B.; Moore, V. C.; Strano, M. S.; Haroz, E. H.; Rialon, K. L.; Boul, P. J.; Noon, W. H.; Ma, J.; Hauge, R. H.; Weisman, R. B.; Smalley, R. E. *Science* **2002**, *297*, 593.
- (5) Bachilo, S. M.; Strano, M. S.; Kittrell, C.; Hauge, R. H.; Smalley, R. E.; Weisman, R. B. *Science* **2002**, *298*, 2361.
- (6) Zoric, Z.; Ostojic, G. N.; Kono, J.; Shaver, J.; Moore, V. C.; Strano, M. S.; Hauge, R. H.; Smalley, R. E.; Wei, X. *Science* **2004**, *304*, 1129.
- (7) Doorn, S. K.; Heller, D. A.; Barone, P. W.; Ursey, M. L.; Strano, M. S. *Appl. Phys. A* **2004**, *78*, 1147.
- (8) Telg, H.; Maultzsch, J.; Reich, S.; Hennrich, F.; Thomsen, C. *Phys. Rev. Lett.* **2004**, *93*, 177401.
- (9) Fantini, C.; Jorio, A.; Souza, M.; Strano, M. S.; Dresselhaus, M. S.; Pimenta, M. A. *Phys. Rev. Lett.* **2004**, *93*, 147406.
- (10) Sfeir, M. Y.; Wang, F.; Huang, L. M.; Chuang, C. C.; Hone, J.; O'Brien, S. P.; Heinz, T. F.; Brus, L. E. *Science* **2004**, *306*, 1540.
- (11) Wang, F.; Dukovic, G.; Brus, L. E.; Heinz, T. F. *Science* **2005**, *308*, 838.
- (12) Maultzsch, J.; Pomraenke, R.; Reich, S.; Chang, E.; Prezzi, D.; Ruini, A.; Molinari, E.; Strano, M. S.; Thomsen, C.; Lienau, C. *Phys. Rev. B* **2005**, *72*, 241402(R).

- (13) Jorio, A.; Fantini, C.; Pimenta, M. A.; Capaz, R. B.; Samsonidze, G. G.; Dresselhaus, G.; Dresselhaus, M. S.; Jiang, J.; Kobayashi, N.; Gruneis, A.; Saito, R. *Phys. Rev. B* **2005**, *71*, 075401.
- (14) Maultzsch, J.; Telg, H.; Reich, S.; Thomsen, C. *Phys. Rev. B* **2005**, *72*, 205438.
- (15) Perebeinos, V.; Tersoff, J.; Avouris, P. *Phys. Rev. Lett.* **2005**, *94*, 027402.
- (16) Thomsen, C.; Reich, S. In *Light Scattering in Solids IX*; Cardona, M., Merlin, R., Eds.; Springer: Berlin, 2006; Chapter 3.
- (17) Popov, V. N.; Henrard, L.; Lambin, P. *Nano Lett.* **2004**, *4*, 1795.
- (18) Popov, V. N.; Henrard, L.; Lambin, P. *Phys. Rev. B* **2005**, *72*, 035436.
- (19) Machon, M.; Reich, S.; Telg, H.; Maultzsch, J.; Ordejon, P.; Thomsen, C. *Phys. Rev. B* **2005**, *71*, 035416.
- (20) Goupalov, S. V. *Phys. Rev. B* **2005**, *71*, 153404.
- (21) Jiang, J.; Saito, R.; Gruneis, A.; Chou, S. G.; Samsonidze, G. G.; Jorio, A.; Dresselhaus, G.; Dresselhaus, M. S. *Phys. Rev. B* **2005**, *71*, 205420.
- (22) Goupalov, S. V.; Satishkumar, B. C.; Doorn, S. K. *Phys. Rev. B* **2006**, *73*, 115401.
- (23) Simon, F.; Kukovecz, A.; Kónya, Z.; Pfeiffer, R.; Kuzmany, H. *Chem. Phys. Lett.* **2005**, *413*, 506.
- (24) Pfeiffer, R.; Simon, F.; Kuzmany, H.; Popov, V. N. *Phys. Rev. B* **2005**, *72*, 161404.
- (25) O'Connell, M. J.; Sivaram, S.; Doorn, S. K. *Phys. Rev. B* **2004**, *69*, 235415.
- (26) Jorio, A.; Fantini, C.; Dantas, M. S. S.; Pimenta, M. A.; Souza Filho, A. G.; Samsonidze, Ge. G.; Brar, V. W.; Dresselhaus, G.; Dresselhaus, M. S.; Swan, A. K.; Unlu, M. S.; Goldberg, B. B.; Saito, R. *Phys. Rev. B* **2002**, *66*, 115411.
- (27) Jorio, A.; Saito, R.; Hafner, J. H.; Lieber, C. M.; Hunter, M.; McClure, T.; Dresselhaus, G.; Dresselhaus, M. S. *Phys. Rev. Lett.* **2001**, *86*, 1118.
- (28) Souza Filho, A. G.; Chou, S. G.; Samsonidze, Ge. G.; Dresselhaus, G.; Dresselhaus, M. S.; An, L.; Liu, J.; Swan, A. K.; Unlu, M. S.; Goldberg, B. B.; Jorio, A.; Gruneis, A.; Saito, R. *Phys. Rev. B* **2004**, *69*, 115428.
- (29) Kataura, H.; Ueno, T.; Miyata, Y.; Yanagi, K.; Okubo, S.; Suzuki, S.; Achiba, Y. Presented at the 20th International Conference on Raman Spectroscopy, Yokohama, Japan, 2006.
- (30) Yee, K. J.; Lee, K. G.; Oh, E.; Kim, D. S.; Lim, Y. S. *Phys. Rev. Lett.* **2002**, *88*, 105501.
- (31) Lee, I. H.; Yee, K. J.; Lee, K. G.; Oh, E.; Kim, D. S.; Lim, Y. S. *J. Appl. Phys.* **2003**, *93*, 4939.
- (32) Aku-Leh, C.; Zhao, J.; Merlin, R.; Menéndez, J.; Cardona, M. *Phys. Rev. B* **2005**, *71*, 205211.
- (33) Rosker, M. J.; Wise, F. W.; Tang, C. L. *Phys. Rev. Lett.* **1986**, *57*, 321.
- (34) Nelson, K. A.; Williams, L. R. *Phys. Rev. Lett.* **1987**, *58*, 745.
- (35) Walmsley, I. A.; Wise, F. W.; Tang, C. L. *Chem. Phys. Lett.* **1988**, *154*, 315.
- (36) Hase, M.; Mizoguchi, K.; Harima, H.; Nakashima, S.; Sakai, K. *Phys. Rev. B* **1998**, *58*, 5448.
- (37) Hodak, J. H.; Henglein, A.; Hartland, G. V. *J. Phys. Chem. B* **2000**, *104*, 9954.
- (38) The CP amplitude in 4b was calculated by taking the peak height of the maxima of the probe profile, assuming it occurs at the inflection point of a Lorentzian function centered at the second excitonic transition for a given  $(n,m)$  semiconducting nanotube with a half width at half maximum of 30 meV, and setting it equal to the expression for the first derivative of the Lorentzian function.
- (39) Jiang, J.; Saito, R.; Samsonidze, Ge. G.; Chou, S. G.; Jorio, A.; Dresselhaus, G.; Dresselhaus, M. S. *Phys. Rev. B* **2005**, *72*, 235408.
- (40) Cardona, M. *Modulation Spectroscopy*; Academic Press: New York, 1969.

NL061599P